From Plots to Landscape: Modeling the Aboveground Biomass of a Conserved Area Using GEDI, LANDSAT, and Topographic Data

Yetunde Rotimi (yetunde.rotimi@wsu.edu)

Introduction

Understanding the benefits that ecosystems provide requires effective tools and techniques that can be used to monitor landscapes over time. Most conserved ecosystems, particularly those designated as forests (e.g., national forests), are known for their critical role in climate regulation through carbon sequestration, mostly stored as aboveground biomass (Baig et al., 2015). This is particularly true if these forests are managed sustainably, as their loss (e.g., deforestation) can make significant contributions to global warming. Ground-based ecosystem assessments of forest biomass often yield the most accurate results; however, the ground-based techniques can be limited by cost, and the inability to provide information over large extents. The development of new monitoring strategies using remote sensing data has proven effective in mapping aboveground biomass through the years (e.g., Hudak et al. 2020). However, more research is needed to understand how the integration of remote sensing data can help improve prediction and mapping accuracy.

Various conserved ecosystems are managed for varying objectives, encompassing management for biodiversity exclusively, management for multiple uses, and no mandate for management. (Bradley et al., 2016). While management status can be expected to influence aboveground biomass, other factors such as structural metrics, climate, elevation, aspects, slope, and soil conditions may also influence biomass attributes in conserved ecosystems (LaRue et al., 2023; Xu et al., 2020). For instance, compared to forest communities where trees have similar crown architectures, forest communities with differences in tree crown sizes and shapes have higher levels of light absorption and stem biomass (Williams et al., 2017). Also, in certain regions such as the United States, temperature varies across latitudes and elevations, and this can have negative or positive impacts on aboveground biomass (Keith et al., 2009). Although, in some conserved areas, climate variables may have more impacts on biomass than soil properties, however, increased biomass is often enhanced by soil fertility (Bennett et al., 2020; Yuan et al., 2019). Accounting for these factors can help determine which ones primarily influence the quantity and quality of aboveground biomass in conserved areas.

To estimate aboveground biomass across ecosystems, scientists have primarily used metrics derived through traditional plot-based measurements or remotely sensed data (Castaño et al., 2024; Liang, González-Roglich, et al., 2023). Traditional plot-based measurements often involve the collection of field data (e.g., wood density, diameter at breast height (DBH), canopy height) which can be used to estimate aboveground biomass density (AGBD). In some countries like the United States, sites are established for the continuous inventory and monitoring of forest data and some of these sites include the Forest Inventory and Analysis (FIA) plots and the National Ecological Observatory Network (Burrill et al., 2018). Although the traditional method of estimating aboveground biomass provides the most accurate results, the process can be time-consuming, expensive, and limited in spatial scale. Also, this method of estimation sometimes requires destructive sampling (direct or destructive methods) such as deforestation, which contradicts the goals of biodiversity conservation (Huynh et al., 2021). Remotely sensed data however can help fill these gaps by providing extensive spatial coverage at landscape (such as airborne and unmanned aerial vehicles, or UAVs) to global (such as satellite and other spaceborne platforms) extents. Mapping the structure of vegetation is enhanced by active remote sensing techniques like lidar (light detection and ranging) and Synthetic Aperture Radar (SAR), which are more sensitive to the biophysical characteristics of vegetation (Duncanson et al., 2020; Liang, Duncanson, et al., 2023).

For aboveground biomass estimation, several studies have explored the application of remote sensing data (Issa et al., 2020). Some of these studies have been focused on estimating aboveground biomass by integrating optical and SAR data (Y. Li et al., 2020). It has been demonstrated that biomass is strongly correlated with optical remotely sensed data from sources like Landsat, SPOT, WorldView-2, Sentinel-2, and their byproducts, vegetation indices, and texture images (Koch, 2010). Additionally, to optimize the potential of the LiDAR, optical, and SAR data for AGB estimation, some studies have concentrated on combining them (Urbazaev et al., 2018). However, some of these datasets like the optical and SAR are usually affected by saturation which is very prominent in ecosystems with highly dense biomass (Joshi et al., 2017). Also, the effective use of datasets from lidar is often dependent on factors ranging from the availability of ancillary ground data, variation in lidar data acquisition, and the adopted analysis methods (Zhao et al., 2011). Since area-based vegetation attributes such as aboveground biomass cannot be directly measured by remote sensing data, ground-based data are usually integrated with their metrics via correlative models for accurate estimation. Some of the models that have been used for aboveground biomass estimation include machine learning algorithms such as decision tree-based models, random forest, and XGBoost which have shown great performances (Dang et al., 2022; Y. Li et al., 2020). With the improvement in remote sensing technologies, the availability of ground-based data, modeling techniques, and the possibility of integrating lidar data with satellites, crucial information about forest productivity can be assessed more effectively.

Recommendations from previous researchers on aboveground biomass estimation indicate the need to continue exploring the potential of models and datasets to improve the accuracy of AGB estimation using remote sensing data. As such, both spaceborne and airborne data have been used for different applications ranging from canopy height and biomass estimation to wildlife biodiversity prediction (Marselis et al., 2022; Potapov et al., 2021). The ability of remote sensing data, particularly lidar to detect individual tree species is also well-documented (W. Li et al., 2012). Forest structural datasets from lidar have also been integrated with field-plot data such as FIA to estimate aboveground biomass (Crockett et al., 2023). However, studies involving the combination of integrated lidar-satellite data and field-based data in estimating aboveground biomass are limited.

In this study, I intend to use spaceborne lidar from NASA's Global Ecosystem Dynamics Instrument (GEDI), which provides near-global (between 51.6°S and 51.6°N latitude) estimates of forest structures. GEDI was launched into space in 2018 and it measures vegetation's 3-dimensional structure through systematic sampling at 25 m spatial resolution or footprint (Dubayah et al., 2020). The suites of forest structure products provided by GEDI include canopy heights, cover, foliage metrics, and aboveground biomass density (AGBD). Specifically, I'll be working with the wall-to-wall canopy height data at 30m ground sampling distance (GSD) which was developed through the integration of GEDI and Landsat analysis-ready data time-series (Potapov et al., 2021). This integrated dataset does not only offer dense observation of canopy height across the globe but also enables the identification of tall canopies with possible high carbon stocks. In addition, I intend to use airborne lidar from the NEON platform. NEON's airborne observatory platform (AOP) uses lidar sensors to generate ecosystem structures such as the height of the top of the canopy (CHM). These datasets are mosaicked onto a spatially uniform grid at 1 m spatial resolution in 1 km by 1 km tiles and the dense spatial sampling makes it possible to characterize and measure the aboveground biomass of the ecosystem. Other datasets that will be considered in this study include indices and byproduct data from Landsat-8 as well as topographic data. All GEDI, Landsat, AOP, and topographic datasets will be integrated with ground-based data from NEON's terrestrial observation system (TOS) to estimate the aboveground biomass of a conserved ecosystem. Specific research questions include:

1) Assessing the correlation between ground-based field data, NEON AOP canopy height data, and the integrated GEDI-LNADSAT canopy height data

2) Assessing the accuracy of integrated Lidar, Landsat 8, and topography data in estimating aboveground biomass

METHODS

STUDY AREA AND DATA

Study Area

The site considered in this study is the Gifford Pinchot National Forest (GPNF), which is a conserved area in Southern Washington (Figure 1) and managed by the United States Forest Service. Covering 1.32 million acres (46.7582° N, 121.4512° W), the GPNF spans the crest of Washington State's South Cascades and spread over multiple glaciers, old-growth forests, high alpine meadows, and numerous volcanic peaks. The forest elevation ranges from 400 feet to the summit of Mount Adams at 12,276 feet, the second-highest point in Washington. Gifford National Forest has a mean annual temperature of 9.2°C (49°F) and it is characterized by warm, dry summers and cool wet winters with approximately 2,225 mm (87.6 in.) of annual precipitation in the form of rain and snow. The protected area datasets for the Pacific Northwest were downloaded from the database of the U.S. Geological Survey (https://www.usgs.gov/programs/gap-analysis-project/science/pad-us-data-download), from which the GPNF dataset was extracted.

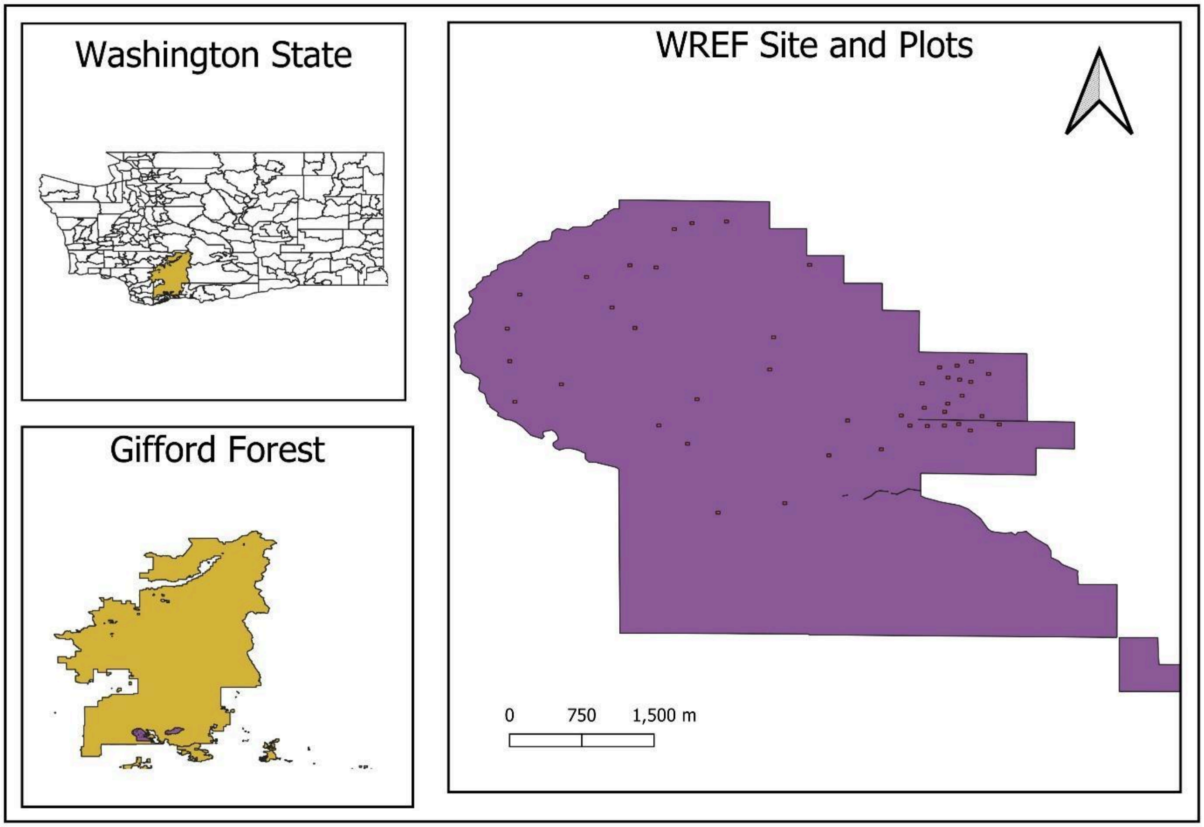

Figure 1: Study Area Location

Field Inventory Data: NEON Terrestrial Observation System (TOS) Data

Located within the old-growth forest of Gifford Pinchot National Forest are the National Ecological Observatory Network plots i.e., the Wind River Experimental Forest (WREF). The Wind River Experimental Forest covers 42 km^2 (10,400 acre) within GPNF and has a rich history of research and timber management since the early 1900s. The area is best known for its old-growth forests of Douglas-fir and western hemlock. Data collection on this site started in 2017 and datasets are gathered from the Terrestrial Observation System (TOS), the Airborne Observation Platform (AOP), the Aquatic Observation System, and the Terrestrial Instrument System (Nagy et al., 2021). WREF site has a total of 86 TOS plots which include the distributed base plots, tower base plots, tick plots, and mammal grids among others. The distributed and tower base plots with a dimension of 40m by 40m are 50 in number, and these are the plots dedicated to vegetation structure measurements. Generally, datasets can be accessed through the

NEON data portal (https://data.neonscience.org/data-products/DP1.10067.001), but for this study, the datasets were obtained using the neonUtilities, neonos, and geoNEON package in R.

Specifically, the vegetation structure data from 2017 – 2021 which contains measurements (stem diameter, height, growth form, etc.) of woody individuals was used for this study. Out of the entire 50 base plots in the site, the extracted datasets only covered 39 plots. In each plot, only trees with height ≥ 3m were considered and, all trees with dead, lost, and downed status were removed. Also, trees with duplicate individual IDs, unknown stem diameters, and unknown heights were removed. Aboveground biomass at the tree level was calculated using species-specific allometric equations (Chojnacky et al., 2014; Jia et al., 2024).

LiDAR Data: Canopy Height Models (CHM)

The canopy height dataset obtained from the integration of Global Ecosystem Dynamics Investigation (GEDI) lidar forest structure measurements and Landsat analysis-ready data time series was used for this study. This dataset was developed by the Global Land Analysis and Discover team at the University of Maryland (UMD GLAD) by integrating the GEDI and Landsat data obtained in 2019. Based on field measurements obtained between 2017 – 2021, the primary conjecture posited that there was no significant variation in woody vegetation attributes between 2017 – 2019 and 2019 – 2021.

The canopy height dataset obtained from the Airborne Observation Platform (AOP) of the WREF site was also considered in this study. The AOP CHM which is generated directly from the lidar point cloud is normalized by ground height to derive the height of vegetation above the ground in meters. The AOP raster for 2019 was used to estimate the mean height of trees in individual 39 plots. The integrated GEDI-Landsat CHM data and AOP CHM data were compared with the field height data to determine correlation. While the CHM dataset from the integration of GEDI and LiDAR has a spatial resolution of 30m, the AOP CHM has a spatial resolution of 1m. Resampling was done to align the spatial resolutions to the size of the plots ($40m^2$).

Landsat 8 Metrics

Landsat metrics which include biomass-related vegetation indices, bands, and data products (Table 1) were downloaded from the Google Earth Engine (GEE) cloud platform. These datasets were integrated with CHM to model aboveground biomass. Specifically, metrics were extracted using Landsat 8 OLI-2 imagery between 2019 and 2021 for the WREF site. Landsat 8 OLI datasets contain four visible, one near-infrared (NIR) band, and two short-wave infrared (SWIR) bands with 30 m resolution, which were resampled to align with the spatial scale of the study area. Cloud masking was applied to the imagery to remove the cloud effect.

Topographic Factors

The topographic factors considered in this study include slope, aspect, and elevation. These datasets were obtained alongside the field vegetation structure data from the NEON site.

Table 1: Independent Variables for Estimating Aboveground Biomass across WREF Site

	Predictors	Description/Formula
LiDAR	GEDI_Landsat_CHM	Canopy height model from integrated GEDI and Landsat data
	AOP_CHM	Canopy height model from NEON AOP
Landsat	Net primary productivity (NPP)	
	Normalized difference vegetation index (NDVI)	(NIR - Red) / (NIR + Red)
	Soil adjusted vegetation index (SAVI)	((NIR - Red) / (NIR + Red + L)) x (1 + L), L = 0.5
	Chlorophyll Index-green (CI)	((NIR)/Green) – 1
	Ratio vegetation index (RVI)	(NIR/Red)
	Difference vegetation index (DVI)	(NIR – Red)
	Wide dynamic range vegetation index (WDRVI)	(((0.1 * NIR) – Red)) / ((0.1 * NIR) + Red)
	Excess green index (ExG)	(2 * Green – Red – Blue)
	Visible atmospherically resistant index (VARI)	(Green – Red) / (Green + Red – Blue)
	Band 2 - 7	Blue, green, red, near-infrared, and short-wave infrared
Topography	Slope	
	Aspect	
	Elevation	

Data Analysis

For this study, a stepwise regression model was adopted for the estimation of aboveground biomass in the study site. Analysis was done in R software using regression model to predict aboveground biomass from the integration of LiDAR, Landsat 8 OLI, and topographic data. The accuracy of aboveground biomass estimation was determined using the root mean square error (RMSE) and R-squared (R^2) values.

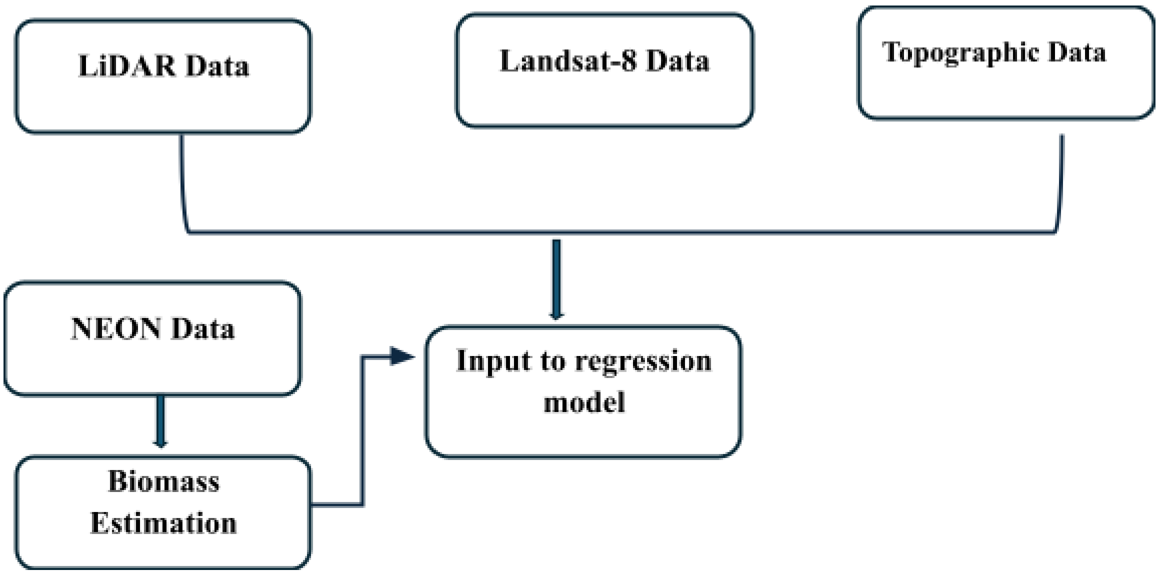

Figure 2: Workflow of aboveground biomass estimation

RESULTS AND DISCUSSION

Field Data Analysis

Results showed that the number of trees on each plot used for this analysis greatly varies, ranging from 5 (plot 9) to 109 (plot 73) and a total of 1,527 trees. A total of 11 species (Figure 3) were identified across plots and the most occurring was *Tsuga heterophylla* (Raf.) Sarg. (651 in total). Next to *Tsuga heterophylla (*Western Hemlock) was *Pseudotsuga menziesii* (Douglas Fir) which occurred 423 times. Like the number of trees per plot, the aboveground biomass also varies ranging from 54.24 (plot 13) – 11012.93 kg/plot (plot 9). Despite having the fewest trees (5 total) of any plot, plot 9 had the highest amount of aboveground biomass conserved (Figure 4), which is explained by the size of the tree stems in the plot. Based on growth form, more single bole trees (1,097) existed on the site compared to multi-bole trees (58), small trees (366), and single shrubs (6). As expected, single-bole trees had the highest aboveground biomass (814kg) compared to the rest of the growth forms. Nonetheless, even though multi-bole trees were less common than small trees, the latter had a larger biomass (326kg) than the former (6.46kg).

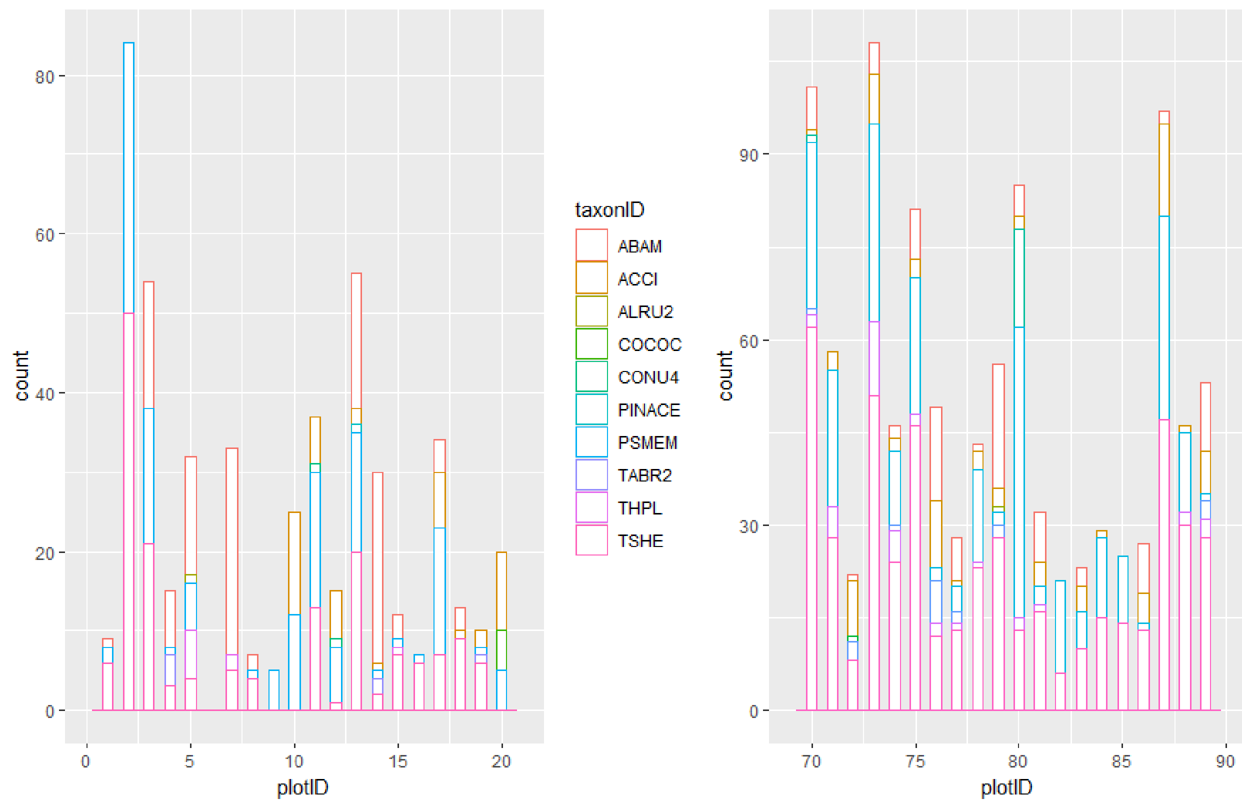

Figure 3: Number of trees per plot and tree species represented.

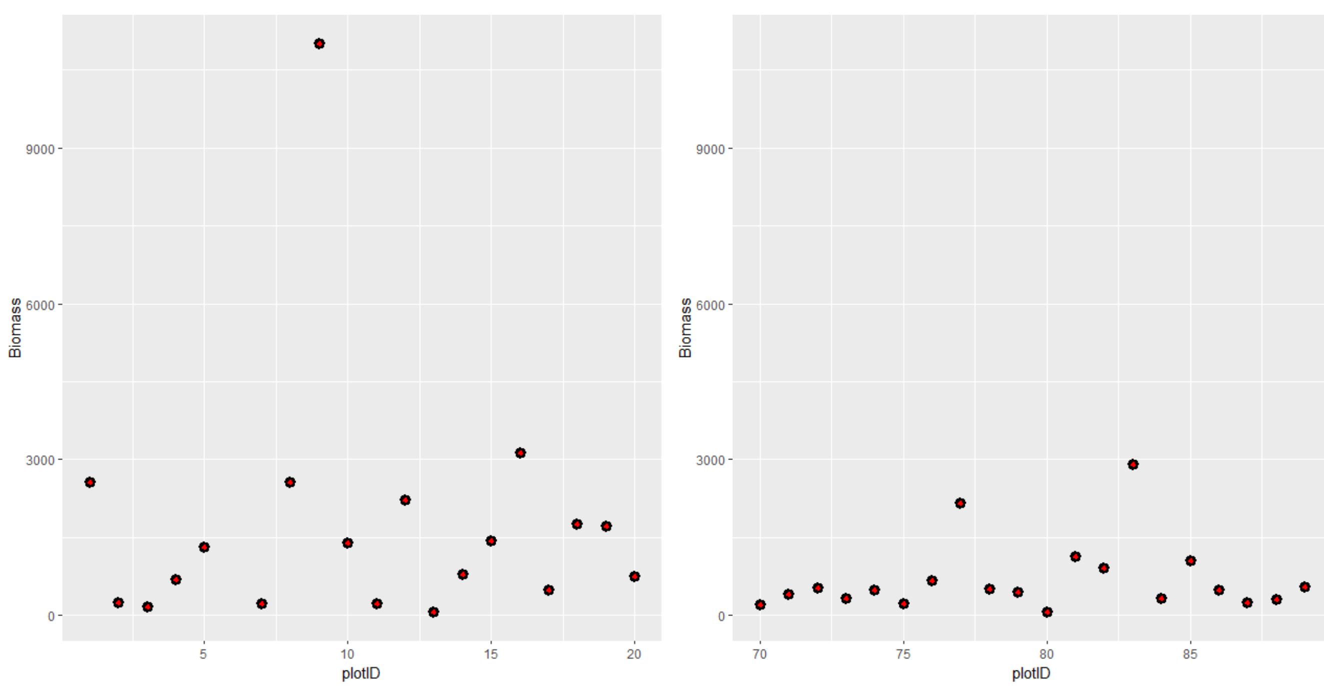

Figure 4: Aboveground biomass (Kg) per plot

Field Height data Vs. Lidar CHMs

Pearson correlation results between the field height and lidar canopy height data showed that the data from the integration of GEDI and Landsat is more correlated (*Pearson cor = 0.44*) to the field height data compared to the AOP data (*pearson cor = 0.2*). The low correlation between the AOP canopy height data and field height data is similar to the findings of (Pau et al., 2022) which showed weak relationships between NEON AOP data and field vegetation metrics such as the Leaf Area Index (LAI) and Canopy Height Model (CHM). The weak correlation could have stemmed from the fact that the tree height data included understory that are not at the top of the canopy which can be easily mapped by lidar data. However, for this analysis, only trees with heights 3 meters and above were considered. Also, the weak correlation could be attributed to the fact that mosaicked NEON products are usually generated from many combined flight lines with changeable flight circumstances (such as brightness) (Chadwick et al., 2020). Therefore, additional corrections such as custom shade masks, atmospheric correction, and topography smoothing might help improve relationships (Chadwick et al., 2020). Results from this study furthermore show the need for ground-validation process when working with NEON AOP data.

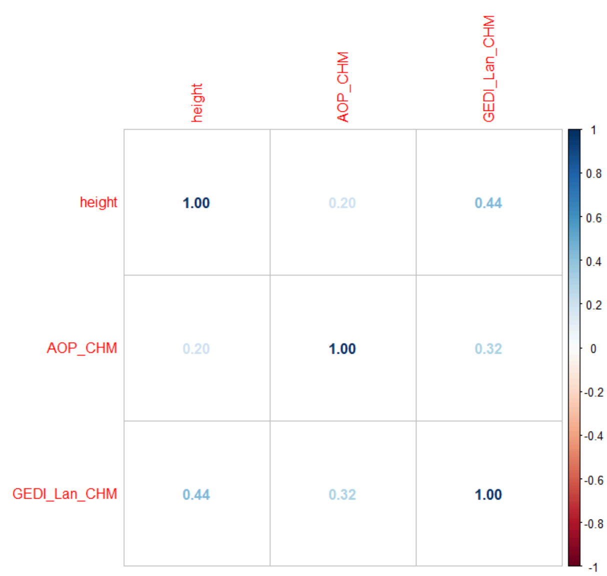

Figure 5: Relationship between field height and Lidar canopy height data

Stepwise Regression Analysis

Using the best model based on AIC (Akaike information criterion) model selection, results showed that 66% of the variation in aboveground biomass could be estimated by the predictor variables. The selected predictor variables included the integrated GEDI/Landsat canopy height data, elevation, one surface reflectance band (Band 5), and five indices. However, the multicollinearity between some of the predictor variables was high (VIF > 10), and as a result, the best significant predictor variables with no multicollinearity were selected. The concluding results showed that only 44% of the variation in aboveground biomass could be estimated by the predictor variables. The final selected predictor variables were the soil-adjusted vegetation index (SAVI), elevation, integrated GEDI/Landsat canopy height data, and net primary productivity (NPP).

While this result showed that integrated Lidar, Landsat metrics, and topographic data can be used to model the aboveground biomass of ecosystems, the estimation accuracy was relatively fair. This result could be attributed to the fact that optical datasets such as Landsat metrics can be easily affected by saturation in ecosystems of highly dense biomass (Tamiminia et al., 2021). Previous analysis by researchers using a combination of Landsat texture images and backscattering coefficients from Sentinel-1 synthetic aperture radar (SAR) under different machine learning algorithms such as XGBoost and random forest (RF) improved estimation accuracy (Y. Li et al., 2020). Optical signals mainly record the horizontal structure of the forest while SAR signals can penetrate the forest canopy and record the vertical structure information. Therefore, using the combination of optical and SAR data to extract parameters for aboveground biomass seems like a promising approach. Nevertheless, one limitation of adopted machine learning algorithms is the decline in model performance for small datasets because of very low subsample ratio that cannot provide enough information to build trees (Freeman et al., 2016). In general, aboveground biomass estimation accuracy may be improved using remote sensing data with better spatial and radiometric resolution, such as LIDAR and hyperspectral data, variable selection, data cleaning, and mixed pixel decomposition.

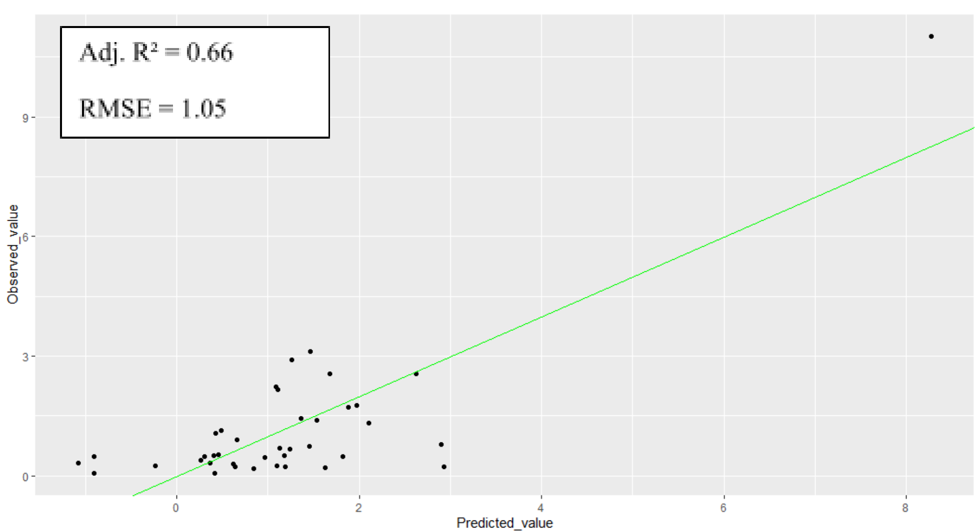

Figure 6: Regression model with selected significant variables (AIC)

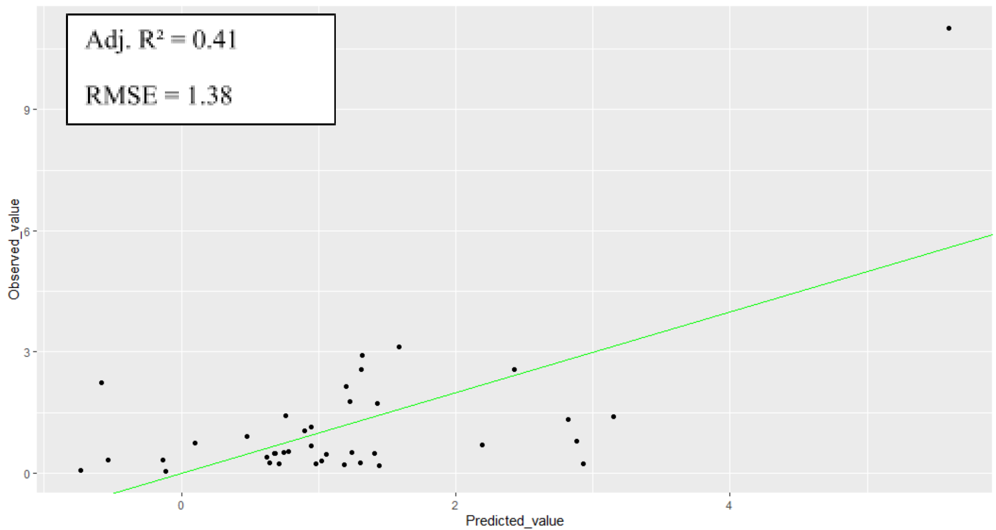

Figure 7: Regression model with the best significant variables

References

Bennett, A. C., Penman, T. D., Arndt, S. K., Roxburgh, S. H., & Bennett, L. T. (2020). Climate more important than soils for predicting forest biomass at the continental scale. *Ecography*, *43*(11), 1692–1705. https://doi.org/10.1111/ecog.05180

Bradley, C. M., Hanson, C. T., & DellaSala, D. A. (2016). Does increased forest protection correspond to higher fire severity in frequent-fire forests of the western United States? *Ecosphere*, *7*(10), e01492. https://doi.org/10.1002/ecs2.1492

Burrill, E. A., Wilson, A. M., Turner, J. A., Pugh, S. A., Menlove, J., Christiansen, G., Conkling, B. L., & David, W. (2018). The Forest Inventory and Analysis Database: Database description and user guide version 8.0 for Phase 2. *US Department of Agriculture, Forest Service*, *946*, 1004.

Castaño, N., Peña, M. A., González-Caro, S., María Aldana, A., Fernanda Casas, L., Correa-Gómez, D. F., González-Abella, J. S., Pelaez, N., Stevenson, P., Sua, S., Zuleta, D., & Duque, Á. (2024). Contrasting drivers of aboveground woody biomass and aboveground woody productivity in lowland forests of Colombia. *Ecography*, *n/a*(n/a), e06693. https://doi.org/10.1111/ecog.06693

Chadwick, K. D., Brodrick, P. G., Grant, K., Goulden, T., Henderson, A., Falco, N., Wainwright, H., Williams, K. H., Bill, M., Breckheimer, I., Brodie, E. L., Steltzer, H., Williams, C. F. R., Blonder, B., Chen, J., Dafflon, B., Damerow, J., Hancher, M., Khurram, A., … Maher, K. (2020). Integrating airborne remote sensing and field campaigns for ecology and Earth system science. *Methods in Ecology and Evolution*, *11*(11), 1492–1508. https://doi.org/10.1111/2041-210X.13463

Chojnacky, D. C., Heath, L. S., & Jenkins, J. C. (2014). Updated generalized biomass equations for North American tree species. *Forestry: An International Journal of Forest Research*, *87*(1), 129–151. https://doi.org/10.1093/forestry/cpt053

Dang, S., Peng, L., Zhao, J., Li, J., & Kong, Z. (2022). A Quantile Regression Random Forest-Based Short-Term Load Probabilistic Forecasting Method. *Energies*, *15*(2), Article 2. https://doi.org/10.3390/en15020663

Dubayah, R., Blair, J. B., Goetz, S., Fatoyinbo, L., Hansen, M., Healey, S., Hofton, M., Hurtt, G., Kellner, J., Luthcke, S., Armston, J., Tang, H., Duncanson, L., Hancock, S., Jantz, P., Marselis, S., Patterson, P. L., Qi, W., & Silva, C. (2020). The Global Ecosystem Dynamics Investigation: High-resolution laser ranging of the Earth's forests and topography. *Science of Remote Sensing*, *1*, 100002. https://doi.org/10.1016/j.srs.2020.100002

Duncanson, L., Neuenschwander, A., Hancock, S., Thomas, N., Fatoyinbo, T., Simard, M., Silva, C. A., Armston, J., Luthcke, S. B., Hofton, M., Kellner, J. R., & Dubayah, R. (2020). Biomass estimation from simulated GEDI, ICESat-2 and NISAR across environmental gradients in Sonoma County, California. *Remote Sensing of Environment*, *242*, 111779. https://doi.org/10.1016/j.rse.2020.111779

Freeman, E. A., Moisen, G. G., Coulston, J. W., & Wilson, B. T. (2016). Random forests and stochastic gradient boosting for predicting tree canopy cover: Comparing tuning processes and model performance. *Canadian Journal of Forest Research*, *46*(3), 323–339. https://doi.org/10.1139/cjfr-2014-0562

Huynh, T., Lee, D. J., Applegate, G., & Lewis, T. (2021). Field methods for above and belowground biomass estimation in plantation forests. *MethodsX*, *8*, 101192. https://doi.org/10.1016/j.mex.2020.101192

Issa, S., Dahy, B., Ksiksi, T., & Saleous, N. (2020). Allometric equations coupled with remotely sensed variables to estimate carbon stocks in date palms. *Journal of Arid Environments*, *182*, 104264. https://doi.org/10.1016/j.jaridenv.2020.104264

Jia, D., Wang, C., Hakkenberg, C. R., Numata, I., Elmore, A. J., & Cochrane, M. A. (2024). Accuracy evaluation and effect factor analysis of GEDI aboveground biomass product for temperate forests in the conterminous United States. *GIScience & Remote Sensing*, *61*(1), 2292374. https://doi.org/10.1080/15481603.2023.2292374

Joshi, C. J., Sharma, D. K., Gotur, M., & Rajan, R. (2017). Effect of Different Chemicals on Seedling Growth and Biomass of Chironji (Buchanania lanzan Spreng.). *International Journal of Current Microbiology and Applied Sciences*, *6*(9), 1819–1823. https://doi.org/10.20546/ijcmas.2017.609.224

Keith, H., Mackey, B. G., & Lindenmayer, D. B. (2009). Re-evaluation of forest biomass carbon stocks and lessons from the world’s most carbon-dense forests. *Proceedings of the*

National Academy of Sciences, *106*(28), 11635–11640. https://doi.org/10.1073/pnas.0901970106

Koch, B. (2010). Status and future of laser scanning, synthetic aperture radar and hyperspectral remote sensing data for forest biomass assessment. *ISPRS Journal of Photogrammetry and Remote Sensing*, *65*(6), 581–590. https://doi.org/10.1016/j.isprsjprs.2010.09.001

LaRue, E. A., Knott, J. A., Domke, G. M., Chen, H. Y., Guo, Q., Hisano, M., Oswalt, C., Oswalt, S., Kong, N., Potter, K. M., & Fei, S. (2023). Structural diversity as a reliable and novel predictor for ecosystem productivity. *Frontiers in Ecology and the Environment*, *21*(1), 33–39. https://doi.org/10.1002/fee.2586

Li, W., Guo, Q., Jakubowski, M. K., & Kelly, M. (2012). A new method for segmenting individual trees from the lidar point cloud. *Photogrammetric Engineering & Remote Sensing*, *78*(1), 75–84.

Li, Y., Li, M., Li, C., & Liu, Z. (2020). Forest aboveground biomass estimation using Landsat 8 and Sentinel-1A data with machine learning algorithms. *Scientific Reports*, *10*(1), 9952. https://doi.org/10.1038/s41598-020-67024-3

Liang, M., Duncanson, L., Silva, J. A., & Sedano, F. (2023). Quantifying aboveground biomass dynamics from charcoal degradation in Mozambique using GEDI Lidar and Landsat. *Remote Sensing of Environment*, *284*, 113367. https://doi.org/10.1016/j.rse.2022.113367

Liang, M., González-Roglich, M., Roehrdanz, P., Tabor, K., Zvoleff, A., Leitold, V., Silva, J., Fatoyinbo, T., Hansen, M., & Duncanson, L. (2023). Assessing protected area's carbon stocks and ecological structure at regional-scale using GEDI lidar. *Global Environmental Change*, *78*, 102621. https://doi.org/10.1016/j.gloenvcha.2022.102621

Pau, S., Nippert, J. B., Slapikas, R., Griffith, D., Bachle, S., Helliker, B. R., O'Connor, R. C., Riley, W. J., Still, C. J., & Zaricor, M. (2022). Poor relationships between NEON Airborne Observation Platform data and field-based vegetation traits at a mesic grassland. *Ecology*, *103*(2), e03590. https://doi.org/10.1002/ecy.3590

Potapov, P., Li, X., Hernandez-Serna, A., Tyukavina, A., Hansen, M. C., Kommareddy, A., Pickens, A., Turubanova, S., Tang, H., Silva, C. E., Armston, J., Dubayah, R., Blair, J. B., & Hofton, M. (2021). Mapping global forest canopy height through integration of GEDI and Landsat data. *Remote Sensing of Environment*, *253*, 112165. https://doi.org/10.1016/j.rse.2020.112165

Tamiminia, H., Salehi, B., Mahdianpari, M., Beier, C. M., Johnson, L., & Phoenix, D. B. (2021). A COMPARISON OF DECISION TREE-BASED MODELS FOR FOREST ABOVE-GROUND BIOMASS ESTIMATION USING A COMBINATION OF AIRBORNE LIDAR AND LANDSAT DATA. *ISPRS Annals of the Photogrammetry, Remote Sensing and Spatial Information Sciences*, *V-3–2021*, 235–241. https://doi.org/10.5194/isprs-annals-V-3-2021-235-2021

Urbazaev, M., Thiel, C., Cremer, F., Dubayah, R., Migliavacca, M., Reichstein, M., & Schmullius, C. (2018). Estimation of forest aboveground biomass and uncertainties by integration of field measurements, airborne LiDAR, and SAR and optical satellite data in Mexico. *Carbon Balance and Management*, *13*(1), 5. https://doi.org/10.1186/s13021-018-0093-5

Williams, L. J., Paquette, A., Cavender-Bares, J., Messier, C., & Reich, P. B. (2017). Spatial complementarity in tree crowns explains overyielding in species mixtures. *Nature Ecology & Evolution*, *1*(4), Article 4. https://doi.org/10.1038/s41559-016-0063

Xu, H., Xiao, J., Zhang, Z., Ollinger, S. V., Hollinger, D. Y., Pan, Y., & Wan, J. (2020). Canopy photosynthetic capacity drives contrasting age dynamics of resource use efficiencies between mature temperate evergreen and deciduous forests. *Global Change Biology*, *26*(11), 6156–6167. https://doi.org/10.1111/gcb.15312

Yuan, Z., Ali, A., Jucker, T., Ruiz-Benito, P., Wang, S., Jiang, L., Wang, X., Lin, F., Ye, J., Hao, Z., & Loreau, M. (2019). Multiple abiotic and biotic pathways shape biomass demographic processes in temperate forests. *Ecology*, *100*(5), e02650. https://doi.org/10.1002/ecy.2650

Zhao, K., Popescu, S., Meng, X., Pang, Y., & Agca, M. (2011). Characterizing forest canopy structure with lidar composite metrics and machine learning. *Remote Sensing of Environment*, *115*(8), 1978–1996. https://doi.org/10.1016/j.rse.2011.04.001